
INTEGRAL PROBABILITY METRIC BASED REGULARIZATION FOR OPTIMAL TRANSPORT

A PREPRINT

Piyushi Manupriya

Department of Computer Science
Indian Institute Of Technology Hyderabad
Kandi, Telangana. INDIA
CS18M20P100002@iith.ac.in

SakethaNath Jagarlapudi

Department of Computer Science
Indian Institute Of Technology Hyderabad
Kandi, Telangana. INDIA
saketha@csce.iith.ac.in

Pratik Jawanpuria

Microsoft IDC, INDIA
pratik.jawanpuria@microsoft.com

June 15, 2022

ABSTRACT

Recently it has been shown that Maximum Mean Discrepancy (MMD) based regularization for optimal transport (OT), unlike the popular Kullback Leibler (KL) based regularization, leads to a dimension-free bound on the sample complexity of estimation. On the other hand, interesting classes of metrics like the Generalized Wasserstein (GW) metrics and the Gaussian-Hellinger-Kantorovich (GHK) metrics are defined using Total Variation and KL based regularizations, respectively. It is, however, an open question if appropriate metrics could be defined using the sample-efficient MMD regularization. In this work, we not only bridge this gap, but further consider a generic family of regularizers based on Integral Probability Metrics (IPMs), which include MMD as a special case. We present novel IPM regularized p -Wasserstein style OT formulations and prove that they indeed induce metrics over measures. While some of these novel metrics can be interpreted as infimal convolutions of IPMs, interestingly, others turn out to be the IPM-analogues of GW and GHK metrics. Finally, we present finite sample-based formulations for estimating the squared-MMD regularized metric and the corresponding barycenter. We empirically study other desirable properties of the proposed metrics and show their applicability in various machine learning applications.

1 Introduction

Optimal transport (OT) has witnessed a lot of success in machine learning applications [38]. OT's success is partly due to clever regularization [13], which plays a critical role in handling noisy marginals [19] or marginals of unequal masses [9, 30], and in affecting the computational complexity [4, 3] as well as the sample complexity [31, 21, 18].

Optimal transport with Kullback Leibler (KL), and in general, ϕ -divergence, based regularization is a very well-understood topic [29, 30, 8, 10, 9]. Regularizers based on Total Variation (TV) are also well-studied [39, 40, 24, 22]. In particular, the Generalized Wasserstein (GW) metrics and the Gaussian-Hellinger-Kantorovich (GHK) metrics are defined using TV and KL based regularizations, respectively. The above works also study some interesting properties of the GW and GHK metrics.

On the other hand, regularization, apart from ϕ -divergence based, has received hardly any attention until recently. Interestingly, [35] showed that Maximum Mean Discrepancy (MMD) [34] based regularization for OT, unlike the popular KL based regularization, leads to a completely dimension-free bound on the sample complexity of estimation. However, it is an open question if appropriate metrics could be defined using the sample-efficient MMD regularization.

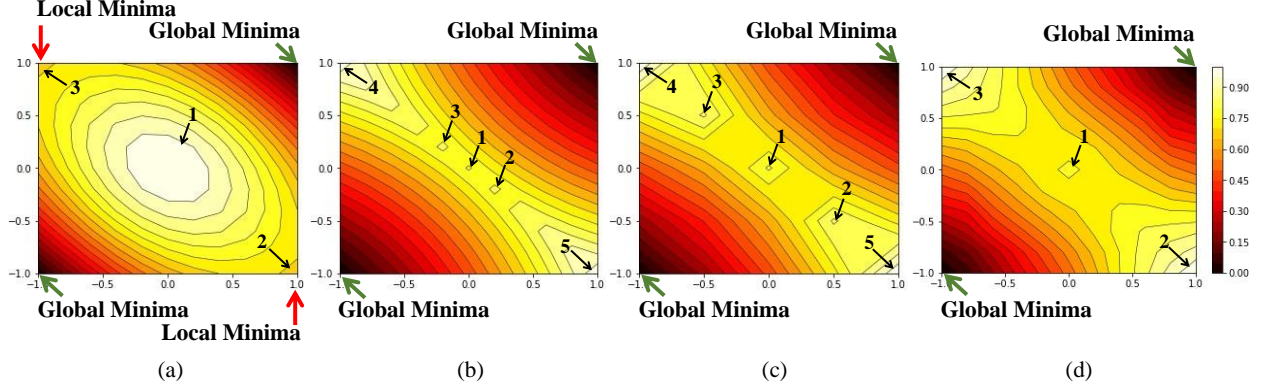


Figure 1: Level sets of distance function between a family of source distributions and a fixed target distribution with the task of finding the source distribution closest to the target distribution (a) MMD (b) OT with no regularization (c) OT with TV regularization (d) OT with proposed MMD regularization. While global minima (marked with Green arrows) is correctly identified by all methods, level sets with the proposed MMD-regularized OT show no local minima (marked with Red arrows) and have lesser number of non-optimal stationary points (marked with Black arrows) compared to (b) and (c). Please refer to Section 4.1 for more details.

In this work we not only provide an affirmative answer to this open question, but also study a more generic family of regularizers based on Integral Probability Metrics (IPMs) [45], which includes MMD as a special case. IPMs are a family of metrics complementary to ϕ -divergences, with the TV metric being the only non-trivial common member. To the best of our knowledge, our work is the first to study IPM regularization in the context of OT.

We begin by proposing a novel family of p -Wasserstein style OT formulations that employ IPM-regularization for matching the marginals. The proposed family subsumes the formulations studied in [39, 40] and [35]. We then focus on two specific settings of the proposed family of OT formulations. The first setting helps us define metrics over measures that can be interpreted as a q -degree infimal convolution of the 1-Wasserstein metric and the IPM employed for regularization. In the special case $q = 1$, we show that these metrics, in fact, belong to the IPM family itself. In the general case (i.e., $q \neq 1$), these metrics do not belong to any previously studied class of metrics. In the second setting, the proposed formulations can be interpreted as p -Wasserstein metrics ($p > 1$) with IPM-regularization. Importantly, under mild conditions, we prove that these IPM-regularized p -Wasserstein metrics are indeed valid metrics. This key result is a non-trivial extension of that in [39, 22], wherein the IPM regularizer is restricted to be the TV. These novel metrics can be understood as the MMD/IPM analogues of the GW/GHK metrics.

Interestingly, the special case of MMD regularized 2-Wasserstein metric seems to be inheriting the desirable properties from its parent metrics while avoiding their inherent limitations. In particular, we prove that the sample complexity of this special case is inherited from the MMD metric (and not from the 2-Wasserstein metric), and hence is dimension free. Following the synthetic setup of [6], we observe in Figure 1 that the proposed metric is better suited for generative modeling than the MMD. Thus, it seems to inherit the loss surface mainly from the 2-Wasserstein metric rather than the MMD metric. For this special case, we present a finite sample-based simplified formulation for estimating the metric. We also present a formulation for solving the corresponding barycenter problem in the finite sample case. These formulations turn out to be instances of convex quadratic programs with non-negative/simplex constraints, which can be solved using projected gradient descent or mirror descent based solvers.

We report the performance of our MMD-regularized 2-Wasserstein metric on ML applications like domain adaptation and class-ratio estimation using benchmark datasets. The results illustrate the efficacy of our methodology compared to existing OT variants. Our results on single-cell RNA sequencing further validate the quality of barycenter interpolation obtained by our approach.

2 Preliminaries

We begin with some notations. Let \mathcal{X} be a set (domain) that forms a compact Hausdorff space. Let $\mathcal{R}^+(\mathcal{X})$, $\mathcal{R}(\mathcal{X})$ denote the set of all non-negative, signed (finite) Radon measures defined over \mathcal{X} ; while the set of all probability measures is denoted by $\mathcal{P}(\mathcal{X})$. For a measure on the product space, $\pi \in \mathcal{R}^+(\mathcal{X} \times \mathcal{X})$, let π_1, π_2 denote the first and second marginals respectively (i.e., they are the push-forwards under the canonical projection maps onto \mathcal{X}). Let $\mathcal{L}(\mathcal{X})$

and $\mathcal{C}(\mathcal{X})$ denote the set of all real-valued measurable functions and all real-valued continuous functions, respectively, over \mathcal{X} .

2.1 Integral Probability Metrics

Given a set $\mathcal{G} \subset \mathcal{L}(\mathcal{X})$, the Integral Probability Metric (IPM) [34, 45, 1], or the dual norm, associated with \mathcal{G} , is defined by:

$$\gamma_{\mathcal{G}}(s_0, t_0) \equiv \max_{f \in \mathcal{G}} \left| \int_{\mathcal{X}} f \, ds_0 - \int_{\mathcal{X}} f \, dt_0 \right| \quad \forall s_0, t_0 \in \mathcal{R}^+(\mathcal{X}). \quad (1)$$

Classical examples of IPMs include:

Kantorovich: Let d be a given (ground) metric over the domain \mathcal{X} . Let, $\|f\|_d \equiv \max_{x \in \mathcal{X} \neq y \in \mathcal{X}} \frac{|f(x) - f(y)|}{d(x, y)}$, denote the Lipschitz constant of f with respect to the metric d . Kantorovich metric is the IPM associated with the generating set: $\mathcal{W}_d \equiv \{f : \mathcal{X} \mapsto \mathbb{R} \mid \|f\|_d \leq 1\}$. From the Kantorovich-Fenchel duality we have that the Kantorovich metric, when restricted to the set of probability measures, $\mathcal{R}_1^+(\mathcal{X})$, is same as the **1-Wasserstein** metric.

Maximum Mean Discrepancy (MMD): Let k be a characteristic kernel [46] over the domain \mathcal{X} . Let $\|f\|_k$ denote the norm of f in the canonical reproducing kernel Hilbert space (RKHS), \mathcal{H}_k , corresponding to k . MMD is the IPM associated with the generating set: $\mathcal{M}_k \equiv \{f \in \mathcal{H}_k \mid \|f\|_k \leq 1\}$.

Total Variation (TV): This is the IPM associated with the generating set: $\mathcal{T} \equiv \{f : \mathcal{X} \mapsto \mathbb{R} \mid \|f\|_{\infty} \leq 1\}$, where $\|f\|_{\infty} \equiv \max_{x \in \mathcal{X}} |f(x)|$.

Dudley: This is the IPM associated with the generating set: $\mathcal{D}_d \equiv \{f : \mathcal{X} \mapsto \mathbb{R} \mid \|f\|_{\infty} + \|f\|_d \leq 1\}$, where d is a ground metric over \mathcal{X} . The so-called **Flat** metric is related to the Dudley metric. Its generating set is: $\mathcal{F}_d \equiv \{f : \mathcal{X} \mapsto \mathbb{R} \mid \|f\|_{\infty} \leq 1, \|f\|_d \leq 1\}$.

Kolmogorov: Let $\mathcal{X} = \mathbb{R}^n$. Then, Kolmogorov metric is the IPM associated with the generating set: $\mathcal{K} \equiv \{1_{(-\infty, x)} \mid x \in \mathbb{R}^n\}$.

In order that the IPM metrizes weak convergence, we assume the following [34]:

Assumption 2.1. \mathcal{G} is dense in $\mathcal{C}(\mathcal{X})$ and is compact.

Since the IPM generated by \mathcal{G} and its absolute convex hull are the same, (without loss of generality) we additionally assume the following:

Assumption 2.2. \mathcal{G} is absolutely convex.

2.2 Optimal Transport

Given a cost function, $c : \mathcal{X} \times \mathcal{X} \mapsto \mathbb{R}$, and two probability measures $s_0 \in \mathcal{R}_1^+(\mathcal{X})$, $t_0 \in \mathcal{R}_1^+(\mathcal{X})$, the p -Wasserstein Kantorovich OT formulation is given by:

$$\bar{W}_p^p(s_0, t_0) \equiv \min_{\pi \in \mathcal{R}_1^+(\mathcal{X} \times \mathcal{X})} \int c^p \, d\pi, \quad \text{s.t. } \pi_1 = s_0, \pi_2 = t_0. \quad (2)$$

An optimal solution of (2) is called as a transport plan. Whenever the cost is a metric, d , over \mathcal{X} (ground metric), \bar{W}_p defines another metric, known as the p -Wasserstein metric, over $\mathcal{R}_1^+(\mathcal{X})$. This has many applications: as a loss function [19], for measure interpolation [23], etc. The Kantorovich-Fenchel duality result shows that the 1-Wasserstein metric is same as the Kantorovich metric, when restricted to probability measures.

In case the given measures, $s_0, t_0 \in \mathcal{R}^+(\mathcal{X})$, it may happen that they are of unequal masses. This is known as the unbalanced optimal transport (UOT) setting. In UOT or when the measures are uncertain (perhaps sample based), one employs a regularized version [30, 8]:

$$\min_{\pi \in \mathcal{R}^+(\mathcal{X} \times \mathcal{X})} \int c \, d\pi + \lambda D_{\phi}(\pi_1, s_0) + \lambda D_{\phi}(\pi_2, t_0), \quad (3)$$

where D_{ϕ} is the divergence generated by ϕ . In the special case D_{ϕ} is the KL divergence and the ground cost c is squared-Euclidean, the optimal objective of (3) is square of the so-called Gaussian Hellinger-Kantorovich metric [30] between the marginals s_0, t_0 .

[40] studied a Total Variation metric (denoted by $|\cdot|_{TV}$) regularized OT formulation:

$$\min_{\pi \in \mathcal{R}^+(\mathcal{X} \times \mathcal{X})} |\pi|^{p-1} \int c^p d\pi + \lambda |\pi_1 - s_0|_{TV}^p + \lambda |\pi_2 - t_0|_{TV}^p, \quad (4)$$

where $|\pi|$ is the mass of measure π . The p^{th} -root of the optimal objective of (4) is the so-called generalized Wasserstein metric between s_0, t_0 .

3 Proposed IPM-regularized OT

In this section, we study the proposed IPM-regularized OT formulations. To begin with, consider the following novel family of OT formulations:

$$(\mathcal{U}_{\mathcal{G},c,\lambda,p,q}(s_0, t_0))^q \equiv \min_{\pi \in \mathcal{R}^+(\mathcal{X} \times \mathcal{X})} \left(|\pi|^{p-1} \int c^p d\pi \right)^{q/p} + \lambda \gamma_{\mathcal{G}}^q(\pi_1, s_0) + \lambda \gamma_{\mathcal{G}}^q(\pi_2, t_0), \quad (5)$$

where $\gamma_{\mathcal{G}}$ is the IPM associated with the generating set, \mathcal{G} , $\lambda > 0$ is the regularization hyperparameter, $|\pi|$ denotes the mass of measure π , and $p \geq 1, q \geq 1$. The above can be equivalently re-written in the following q -degree infimal convolutional form:

$$(\mathcal{U}_{\mathcal{G},c,\lambda,p,q}(s_0, t_0))^q = \min_{s,t \in \mathcal{R}^+(\mathcal{X})} |s|^q (W_p(s, t))^q + \lambda \gamma_{\mathcal{G}}^q(s, s_0) + \lambda \gamma_{\mathcal{G}}^q(t, t_0), \quad (6)$$

where $W_p(s, t) \equiv \begin{cases} \bar{W}_p(\frac{s}{|s|}, \frac{t}{|t|}) & \text{if } |s| = |t|, \\ \infty & \text{otherwise.} \end{cases}$

In the special case $p = q$ or $q = 1$, and \mathcal{G} is the unit ∞ -norm ball, \mathcal{U} recovers the generalized Wasserstein metric, (4). As far as we know, it is an open question if \mathcal{U} is a metric for arbitrary generating sets and in particular, the sample-efficient MMD metric. We fill this gap in literature by analyzing metric properties of (5) and (6) with general \mathcal{G} in two special cases: the case of $p = 1$ is presented in Section 3.1 and that of $p > 1$ is presented in Section 3.2. The proofs of all the results are provided in the supplementary material.

3.1 Case: $p = 1$

The metric property in this case is given by the following theorem:

Theorem 3.1. *Let \mathcal{G} satisfy Assumption 2.1, then $\gamma_{\mathcal{G}}$ is a valid IPM. Let c be a ground metric over \mathcal{X} and $\lambda > 0, q \geq 1$. Then, $\mathcal{U}_{\mathcal{G},c,\lambda,1,q}$ is a norm induced metric over $\mathcal{R}^+(\mathcal{X})$.*

The proof of this theorem critically uses the convexity of W_1 and convexity of IPMs.

Remark 3.2. In general, when the IPM is not the TV metric, and $q > 1$, the proposed metrics $\mathcal{U}_{\mathcal{G},c,\lambda,1,q}$ do not belong to any known class of metrics over measures.

In the case $q = 1$, as shown in the following theorem, the metrics $\mathcal{U}_{\mathcal{G},c,\lambda,1,1}$ belong to the IPM family:

Theorem 3.3. *Whenever \mathcal{G} satisfies Assumptions 2.1 and 2.2, c is a (continuous) ground metric over compact \mathcal{X} , and $\lambda > 0$, we have that:*

$$\mathcal{U}_{\mathcal{G},c,\lambda,1,1}(s_0, t_0) = \max_{f \in \mathcal{G}(\lambda) \cap \mathcal{W}_c} \int_{\mathcal{X}} f ds_0 - \int_{\mathcal{X}} f dt_0. \quad (7)$$

Here, $\mathcal{G}(\lambda) \equiv \{\lambda g \mid g \in \mathcal{G}\}$ and \mathcal{W}_c is all 1-Lipschitz functions wrt. metric c .

The theorem follows by deriving the Fenchel dual of (5) in the special case $p = q = 1$.

Remark 3.4. If \mathcal{G} is the unit uniform-norm ball (corresponding to TV), our result specializes to that in [40], which proves that \mathcal{U} coincides with the so-called Flat metric (or the bounded Lipschitz distance).

Remark 3.5. If the regularizer is the Kantorovich metric¹, i.e., $\mathcal{G} = \mathcal{W}_c$, and $\lambda \geq 1$, then $\mathcal{U}_{\mathcal{W}_c,c,\lambda,1,1}$ coincides with the Kantorovich metric. In other words, the Kantorovich-regularized OT is same as the Kantorovich metric. Thus, our proposed formulation (5) provides the OT interpretation for the Kantorovich metric, which is valid for all (potentially un-normalized) measures in $\mathcal{R}^+(\mathcal{X})$.

¹The ground metric in \mathcal{U} must be same as that defining the Kantorovich regularizer.

3.2 Case: $p > 1$

This is perhaps a more interesting case because it includes the regularized version of the popular 2-Wasserstein metric, which has been shown to induce useful geometries [6]. Also, it is a far more challenging case to analyse as the metrics W_p for $p > 1$ need not be convex. Hence the proof strategy of the earlier case does not apply. Interestingly, under some mild conditions, we show the metric properties even when $p > 1$ with general IPM-regularizers:

Theorem 3.6. *Let \mathcal{G} satisfy Assumption 2.1, then $\gamma_{\mathcal{G}}$ is a valid IPM. Further assume that $\max_{g \in \mathcal{G}} \|g\|_{\infty} = \beta$. Let the cost c be a metric that is bounded i.e., $0 < r \leq c(x, y) \leq R \forall x, y \in \mathcal{X}$. Let $p > 1, q = 1$ and $\lambda \leq \frac{r^p}{pR^{p-1}\beta}$. Then, $\mathcal{U}_{\mathcal{G},c,\lambda,p,1}$, defined in (5), is a metric over $\mathcal{R}^+(\mathcal{X})$.*

The proof is technical and is inspired from gluing lemma style arguments.

Remark 3.7. The existence of β, r, R are indeed mild assumptions. For example, if the IPM is the MMD induced by the Gaussian kernel, then $\beta = 1$. Also, if the measures are discrete or sample-based, then r, R can be computed in a straight-forward manner.

Remark 3.8. The bound on λ can be improved by making more assumptions. For e.g., by additionally assuming $\exists \alpha > 0 \ni \gamma_{\mathcal{G}}(s, t) \geq \alpha|s - t|_{TV} \forall s, t \in \mathcal{R}^+(\mathcal{X})$, the bound improves to $\frac{r^p}{pR^{p-1}(\beta-\alpha)}$. However, some upper bound on λ seems to be intrinsic rather than an artifact of the proof. For e.g., such an upper bound exists for the GHK metrics [30] too. Even in practice, very high λ essentially ignores the transport cost term, rendering the formulation meaningless.

Remark 3.9. In general, whenever \mathcal{G} is not the unit uniform-norm ball, the metrics, $\mathcal{U}_{\mathcal{G},c,\lambda,p,1}$, do not belong to any existing class of metrics over measures. In the case \mathcal{G} is the unit uniform-norm ball, $\mathcal{U}_{\mathcal{T},c,\lambda,p,1}$, coincides with the GW metrics [39].

In summary, we presented two different classes of novel metrics: $\mathcal{U}_{\mathcal{G},c,\lambda,p,1}, p > 1$ and $\mathcal{U}_{\mathcal{G},c,\lambda,1,q}, q \geq 1$. Unlike existing classes of regularized OT metrics, the key advantage is that our metrics include the sample-efficient MMD regularization. A close observation of [35]’s proof strategy shows that the MMD regularized OT inherits its dimension-free sample complexity from that of MMD. Generalizing this result, we present the following theorem:

Theorem 3.10. *Consider $\mathcal{U}_{\mathcal{G},c,\lambda,p,1}$, defined in (5), in the special case of balanced OT, i.e., $|s_0| = |t_0| = 1$ and $\pi \in \mathcal{R}_1^+(\mathcal{X} \times \mathcal{X})$. Let us denote $\mathcal{U}_{\mathcal{G},c,\lambda,p,1}$ in this special case by $\bar{\mathcal{U}}$. Let \hat{s}_m, \hat{t}_m denote the empirical estimates of s_0, t_0 respectively with m samples. Then, $\bar{\mathcal{U}}(\hat{s}_m, \hat{t}_m) \rightarrow \bar{\mathcal{U}}(s_0, t_0)$ at a rate same as that of $\gamma_{\mathcal{G}}(\hat{s}_m, s_0) \rightarrow 0$.*

3.3 Finite Sample Simplifications

Encouraged by the above theoretical results, we now focus on few pragmatic details for employing the proposed metrics in machine learning (ML) applications. For the sake of simplicity of presentation, we consider the following MMD regularized variant in this section:

$$\mathcal{U}(s_1, s_2) \equiv \min_{\pi \in \mathcal{R}^+(\mathcal{X} \times \mathcal{X})} \int c^2 d\pi + \lambda_1 \|\mu_{\pi_1} - \mu_{s_1}\|^2 + \lambda_2 \|\mu_{\pi_2} - \mu_{s_2}\|^2, \quad (8)$$

Here, $\mu_s \equiv \int \phi(x) ds(x)$ is the kernel mean embedding of s [33], ϕ is the canonical feature map, and $\|\cdot\|$ denotes the RKHS norm associated with a given characteristic kernel k .

In typical ML applications, only samples from s_i are available. Accordingly, the support of the optimal plan is assumed to be finite/fixed and estimation is performed. Let m_i samples from s_i be given: $\mathcal{D}_i = \{x_{i1}, \dots, x_{im_i}\}$. Let us denote the Gram-matrix of \mathcal{D}_i by G_{ii} . Let \mathcal{C}_{12} be the $m_1 \times m_2$ cost matrix with entries as evaluations of function c^2 over $\mathcal{D}_1 \times \mathcal{D}_2$. As mentioned earlier, let us assume the transport plan is supported only at the samples²: let $\alpha_{ij} \equiv \pi(x_{1i}, x_{2j})$. Then, $\mu_{\pi_1} = \frac{1}{m_1} \sum_{i=1}^{m_1} \sum_{j=1}^{m_2} \alpha_{ij} \phi(x_{1i})$, $\mu_{\pi_2} = \frac{1}{m_2} \sum_{j=1}^{m_2} \sum_{i=1}^{m_1} \alpha_{ij} \phi(x_{2j})$ and the estimate of μ_{s_i} is $\frac{1}{m_i} \sum_{j=1}^{m_i} \phi(x_{ij})$. With this notation, (8) simplifies as:

$$\min_{\alpha \geq 0 \in \mathbb{R}^{m_1 \times m_2}} \text{Tr}(\alpha \mathcal{C}_{12}^{\top}) + \lambda_1 \|\alpha \mathbf{1} - \frac{\sigma_1}{m_1} \mathbf{1}\|_{G_{11}}^2 + \lambda_2 \|\alpha^{\top} \mathbf{1} - \frac{\sigma_2}{m_2} \mathbf{1}\|_{G_{22}}^2, \quad (9)$$

where $\text{Tr}(M)$ denotes the trace of matrix M and $\|x\|_M^2 \equiv x^{\top} M x$.

A related problem is that of barycenter interpolation of measures [2], which has interesting applications [44, 43, 23]. Given measures s_1, \dots, s_n with total masses $\sigma_1, \dots, \sigma_n$ respectively, and interpolation weights ρ_1, \dots, ρ_n , the

²We can also assume the support is $\mathcal{D}_1 \cup \mathcal{D}_2$ on both sides.

barycenter $s \in \mathcal{R}^+(X)$ is defined as the solution of

$$\min_{s \in \mathcal{R}^+(X)} \sum_{i=1}^n \rho_i \mathcal{U}(s_i, s). \quad (10)$$

In typical ML applications, only sample sets, \mathcal{D}_i , from s_i are available instead of s_i themselves. Following [14] and other related works, we assume³ that the barycenter, s , is supported by $\cup_{i=1}^n \mathcal{D}_i$ and $\beta \in \mathbb{R}^m$ denotes the corresponding probabilities. Here, $m = \sum_{i=1}^n m_i$. Accordingly, we assume that the transport plan π^i corresponding to $\mathcal{U}(s_i, s)$ is supported by $\mathcal{D}_i \times \cup_{i=1}^n \mathcal{D}_i$ and let $\alpha_i \geq 0 \in \mathbb{R}^{m_i \times m}$ denote the corresponding probabilities. Let us denote the Gram-matrix of $\cup_{i=1}^n \mathcal{D}_i$ by G . Let \mathcal{C}_i be the $m_i \times m$ matrix with entries as evaluations of cost function, c^2 . Then, the proposed barycenter formulation (10) simplifies as:

$$\min_{\alpha_i, \beta \geq 0} \sum_{i=1}^n \rho_i \left\{ \text{Tr}(\alpha_i \mathcal{C}_i^\top) + \lambda_1 \|\alpha_i \mathbf{1} - \frac{\sigma_i}{m_i} \mathbf{1}\|_{G_i}^2 + \lambda_2 \|\alpha_i^\top \mathbf{1} - \beta\|_G^2 \right\}.$$

The minimization with respect to β is a standard weighted least-squares problem, which gives the analytical solution: $\beta = \sum_{j=1}^n \rho_j \alpha_j^\top \mathbf{1}$. Using this to eliminate β , leads to

$$\min_{\alpha_i \geq 0} \sum_{i=1}^n \rho_i \left(\text{Tr}(\alpha_i \mathcal{C}_i^\top) + \lambda_1 \|\alpha_i \mathbf{1} - \frac{\sigma_i}{m_i} \mathbf{1}\|_{G_i}^2 + \lambda_2 \|\alpha_i^\top \mathbf{1} - \sum_{j=1}^n \rho_j \alpha_j^\top \mathbf{1}\|_G^2 \right). \quad (11)$$

Problems (9), (11) are instances of convex quadratic programs with non-negativity constraints. In the setting where all involved measures are normalized, the non-negativity constraints can be replaced by simplex constraints. In either case, they can be solved using the mirror-descent algorithm.

4 Experiments

We empirically evaluate the proposed MMD regularized (unbalanced) OT formulation (9) on synthetic as well as real-world datasets. On synthetic datasets, we compare against the 2-Wasserstein, Generalized Wasserstein (GW-TV) [40] and MMD baselines. We also compared our approach with KL-divergence regularized unbalanced OT formulation with entropy regularization [9] (ϵ KL-UOT) and MMD metric on machine learning (ML) applications.

For experiments with the proposed MMD regularized formulation, we either use the characteristic Gaussian (RBF) kernel with $k(x, y) = \exp(-\frac{\|x-y\|_2^2}{2\sigma^2})$ for some $\sigma > 0$ or the characteristic Inverse Multi-Quadratic (IMQ) kernel with $k(x, y) = (K^2 + \|x-y\|_2^2)^{-0.5}$ for some $K > 0$ [47]. For GW-TV, we show qualitative results only with $p = 1$ case (solved using Linear Programming) due to computational constraints. More experimental details and results are in the supplementary material.

4.1 Synthetic Experiments

4.1.1 Level set of distances between distributions

Dataset and experimental setup. Similar to [6], we consider a model family for source distributions as $\mathcal{F} = \{P_\theta = \frac{1}{2}(\delta_\theta + \delta_{-\theta}) : \theta \in [-1, 1] \times [-1, 1]\}$ and a fixed target distribution Q as $P_{(2,2)} \notin \mathcal{F}$. We show distances between P_θ and Q on varying θ .

Compared Methods. Figure 1 presents level sets showing distances $\{d(P_\theta, Q) : \theta \in [-1, 1] \times [-1, 1]\}$ where the distance $d(\cdot, \cdot)$ is measured using MMD, 2-Wasserstein, GW-TV and the proposed OT regularized formulations respectively.

Parameter tuning and evaluation protocol. Applications like generative modeling deal with optimization over parameter (θ) of the source distribution to match the target distribution. In such a case, level sets showing lesser number of stationary points which are not global optima are desirable.

For MMD, RBF kernel is used with σ^2 as 3. Level sets of 2-Wasserstein (OT with no regularization) with squared-Euclidean ground metric are shown. Level sets of GW-TV have Euclidean distance as the ground metric and λ as 10. For the proposed method, the chosen hyper-parameters are: squared-Euclidean cost as the ground metric, λ as 10, squared-MMD regularization and RBF kernel with σ^2 as 2. MMD and the proposed method are solved using the mirror descent algorithm.

³Analogous derivations can be done with any other such finite parameterizations too.

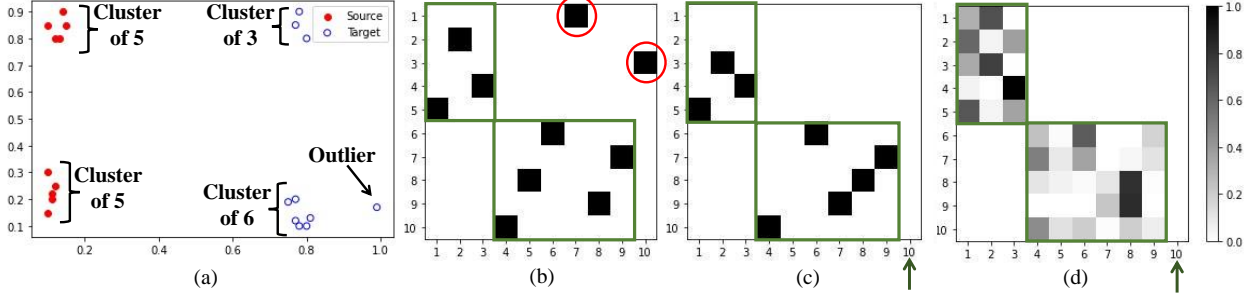


Figure 2: (a) Both the source and the target data are clustered into two groups and the target has an additional outlier. Figures (b), (c), and (d) are the transport plans learned using OT with no regularization, GW-TV, and the proposed approach (9), respectively. Plans (c) and (d) leave the outlier uncoupled (green arrow), and have the expected block diagonal structure (outlined in green). Since (c) is aggressively sparse, the proposed (d) is most suitable.

Results. Figure 1 demonstrates that the level sets of MMD show spurious local minima. The level sets of Wasserstein (OT with no regularization) and GW-TV (TV regularized) show more number of local maxima's compared to the level sets with the proposed approach.

4.1.2 Transport plan in outlier-setting

Dataset and experimental setup. The data is presented in Figure 2(a). Both the source and the target data points are clustered into two groups. Additionally, the last data point of the target data is an outlier. In this set-up, the transport plan between the source and target is expected to have a block diagonal structure with the last column as all zeros.

Compared Methods. We compare the transport matrices of Wasserstein (OT with no regularization), GW-TV (OT with TV regularization) and the proposed approach (9).

Parameter tuning and evaluation protocol. For all the methods, Euclidean distance metric is taken as ground cost. For GW-TV, λ is chosen as 0.4. The proposed method is solved using Mirror Descent, λ is chosen as 0.1, MMD regularization is employed with RBF kernel and σ^2 as 10^{-3} . The regularization coefficients of GW-TV and the proposed approach have been chosen high enough.

Results. As shown in Figure 2, the transport matrix of the proposed approach (9) correctly captures this structure. The transport matrix of the Wasserstein formulation fails to do this and the transport matrix of GW-TV shows some block-diagonal structure but is aggressively sparse.

4.2 Single cell RNA sequencing

Single cell RNA sequencing technique (scRNA-seq) provides insights into cellular functionality by recording expression profiles of genes [27, 51]. An expression profile is a mathematical expression of cells as vectors in gene expression space, where each dimension corresponds to gene. scRNA-seq helps us understand how the expression profile of the cells change over stages [41]. A population of cells is represented as a measure on the gene expression space and as they grow/divide/die and the measure evolves over time. While scRNA-seq records such a measure at a time stamp, it does so by destroying the cells [41]. Thus, it is not possible to monitor how the cell population evolve continuously over time. In fact, only a few measurements at discrete timesteps are generally taken due to the cost involved. Barycenter estimation in the OT framework offers a principled approach to estimate the trajectory of a measure at an intermediate timestep t ($t_i < t < t_j$) when we have measurements available only at t_i (source) and t_j (target) time steps.

Dataset and experimental setup. We perform experiments on the Embryoid Body (EB) single-cell dataset [32]. The dataset has samples available at five timesteps (t_j with $j = 0, \dots, 4$) which were collected during a 25-day period of development of human embryo. Following [49], we project the data onto two-dimensional space and associate uniform measures to the source and the target samples given at different timesteps. We consider the samples at timestep t_i and t_{i+2} as the samples from the source and target measures where $0 \leq i \leq 2$ and aim at estimating the measure at t_i timestep as their barycenter with equal interpolation weights $\rho_1 = \rho_2 = 0.5$.

Compared methods. The barycenter of the measures are computed using the proposed MMD-UOT (11) and the ϵ KL-UOT [8, 30] approaches. For both, simplex constraint is used to cater to the case of uniform measures. The ground metric is taken as squared-Euclidean distance and the IMQ kernel is used as characteristic kernel for MMD-UOT. We

Table 1: EMD (lower is better) between computed barycenter and ground truth distribution

TIMESTEP	MMD	ϵ KL-UOT	PROPOSED
T1	0.045	0.028	0.020
T2	0.012	0.011	0.011
T3	0.009	0.018	0.008

also compare against the empirical average of the source and target measures which is the barycenter obtained with the MMD metric.

Parameter tuning and evaluation protocol. The computed barycenter is evaluated against the measure corresponding to the ground truth samples available at the corresponding timestep. We compute the distance between two using the Earth Mover Distance (EMD). The hyper-parameters are chosen based on leave-one-out validation protocol. For ϵ KL-UOT, the chosen hyper-parameters (λ, ϵ) where λ is the coefficient of KL regularization and ϵ is the coefficient of entropic regularization are: $(1, 10^{-5})$, $(1, 10^{-3})$, $(10^{-2}, 10^{-1})$ at timesteps t_1, t_2, t_3 respectively. For the proposed method, the coefficient of squared-MMD regularization (λ) is chosen as 0.1 and the constant K^2 used in the IMQ kernel is chosen as 10^{-3} at all timesteps.

Results. We observe in Table 1 that the proposed approach performs better than the baselines on all the timesteps, suggesting its superior quality of interpolation.

4.3 Class ratio estimation

We next consider the class ratio estimation problem [26]. Given a multi-class labeled training dataset $L := \{x_i, y_i\}_{i=1}^{m_1}$, the aim is to estimate the ratio of classes in an unlabeled test dataset $U := \{x_j\}_{j=m_1+1}^{m_2}$ (in the same input/output space). Here, $x \in \mathbb{R}^d$ and $y \in Y$, where $Y = \{1, \dots, c\}$ is the set of all labels. It should be noted that the distribution of classes in the labeled dataset may be different from the unlabeled dataset. Thus, while $P_L(y) \neq P_U(y)$, following existing works [52, 26], we assume that $P(x|y)$ remains unchanged across datasets. Lets assume an unknown $\theta \in \Delta_c$, where $\Delta_c := \{z \in \mathbb{R}^c | z \geq \mathbf{0}; \sum_i z_i = 1\}$, is the class ratio in the test dataset, i.e, $P_U(y) = \theta$. Then, a distribution $Q(x) = \sum_{i=1}^c P_L(x|y=i)\theta_i$ should match the test distribution $P_U(x)$.

Existing works [52, 26] use IPMs such as MMD to learn the distribution θ . For solving the class ratio estimation problem with MMD, the formulation is

$$\min_{\theta \in \Delta_c} \frac{1}{m_2} \mathbf{1}^\top G_{11} \mathbf{1} + z(\theta)^\top G_{22} z(\theta) - 2 \frac{1}{m_2} \mathbf{1}^\top G_{12} z(\theta),$$

where $z(\theta) \in \mathbb{R}^{m_1}$, $z_i(\theta) = \frac{\theta_{y_i}}{n_{y_i}}$, and n_j denotes the number of instances labeled j in L and we denote the Gram matrices over the test data and the train data as G_{11}, G_{22} respectively. G_{12} denotes the kernel matrix between the test and train data.

To estimate the class ratios, we employ OT-based metrics with source as the unlabeled test data and target as the labeled train data. A key advantage of IPM-based regularization over KL-based regularization is flexibility in parameterization for estimation. Taking support of the transport matrix as the union of source and target data, we employ the proposed squared-MMD regularized UOT formulation as follows:

$$\min_{\theta \in \Delta_c} \min_{\alpha \in \mathbb{R}^{m_1 \times m_2}, \alpha \geq \mathbf{0}, \mathbf{1}^\top \alpha \mathbf{1} = 1} \text{Tr}(\alpha \mathcal{C}^\top) + \lambda \left(\mathbf{1}^\top \alpha^\top G \alpha \mathbf{1} + \frac{1}{m_2} \mathbf{1}^\top G_{11} \mathbf{1} - 2 \frac{1}{m_2} \mathbf{1}^\top [G_{11} G_{12}] \alpha \mathbf{1} \right) + \lambda \left(\mathbf{1}^\top \alpha G \alpha^\top \mathbf{1} + z(\theta)^\top G_{22} z(\theta) - 2 z(\theta)^\top [G_{21} G_{22}] \alpha^\top \mathbf{1} \right),$$

where \mathcal{C} and G are the cost and the Gram matrices, respectively, over the union of source and target data. The ϵ KL-UOT formulation for class-ratio estimation problem is as follows:

$$\min_{\theta \in \Delta_c} \min_{\substack{\alpha \in \mathbb{R}^{m_1 \times m_2}, \\ \alpha \geq \mathbf{0}, \mathbf{1}^\top \alpha \mathbf{1} = 1}} \text{Tr}(\alpha \mathcal{C}_{12}^\top) + \lambda K L(\alpha \mathbf{1}, \frac{1}{m_2} \mathbf{1}) + \lambda K L(\alpha^\top \mathbf{1}, z(\theta)) + \epsilon \sum_{i=1}^{m_1} \sum_{j=1}^{m_2} \alpha_{i,j} \log \alpha_{i,j}.$$

Dataset and experimental setup. We follow the experimental setup described in [26] and show results on four binary classification datasets from the UCI repository [16]. The fraction of positive class examples on the training set is fixed as 0.5. For each dataset, we create four test set with the fraction of positive class examples as $[0.2, 0.4, 0.6, 0.8]$.

Table 2: Mean Absolute Deviation (lower is better) averaged across test splits

DATASET	MMD	ϵ KL-UOT	PROPOSED
IONOSPHERE	0.106	0.212	0.116
SAHEART	0.169	0.102	0.085
DIABETES	0.171	0.134	0.112
AUSTRALIAN	0.175	0.114	0.089

Table 3: Target accuracy (higher is better) in JUMBOT framework

TASK	ϵ KL-UOT	PROPOSED
DIGITS $U \mapsto M$	98.3	98.4
DIGITS $S \mapsto M$	98.8	97.6
DIGITS $M \mapsto MM$	96.1	96.2
VISDA TRAIN \mapsto VAL	70.9	72.2

Parameter tuning and evaluation protocol. We report the average absolute deviation of the predicted class-ratios from the ground truth. We randomly generate train and test sets, where, for every train set, four test sets are generated corresponding to the four test class-ratios. Hyper-parameters are tuned separately for each class ratio using 30 validation sets that were randomly sampled from the training set. We repeat the whole setup with four random seeds.

Results. The results, averaged across the four test set splits, are reported in Table 2. We observed that the proposed approach performs better than baselines on most datasets.

4.4 Domain Adaptation in JUMBOT framework

OT has been widely employed in domain adaptation problems [12, 11, 42, 15]. JUMBOT [17] is an OT based state-of-the-art domain adaptation method. JUMBOT’s loss function involves a cross entropy term and ϵ KL-UOT discrepancy term between the source and target distributions. We showcase the utility of our MMD-regularized UOT formulation (9) in the JUMBOT [17] framework.

Dataset and experimental setup We perform the domain adaptation experiment with VisDA 2017 [37] and Digits datasets comprising of MNIST [28], M-MNIST [20], SVHN [36], USPS [25] datasets. We replace the ϵ KL-UOT based loss with the proposed MMD-regularized UOT loss (9), keeping the other experimental set-up same as JUMBOT. We obtain JUMBOT’s result with ϵ KL-UOT with the best reported hyper-parameters [17]. Following JUMBOT, we tune our (MMD-regularized UOT loss) hyper-parameters for the Digits experiment on USPS to MNIST ($U \mapsto M$) domain adaptation task and use the same hyper-parameters for SVHN to MNIST ($S \mapsto M$) and MNIST to MMNIST ($M \mapsto MM$) domain adaptation tasks. Following JUMBOT, we report validation accuracy on VisDA 2017.

The chosen hyper-parameters for Digits experiment are IMQ kernel with constant K^2 as 10, λ as 10 and MMD regularization. For VisDA experiment, the chosen hyper-parameters are Gaussian kernel with constant σ^2 as 60, λ as 10 and squared-MMD regularization.

Results Table 3 reports the accuracy obtained on target datasets. We observe that our MMD-regularized UOT loss performances better than ϵ KL-UOT based loss on three out of four datasets.

5 Conclusion

The OT literature seems to have an overwhelming number of results with ϕ -divergence based regularization. In comparison, IPM based regularization has received hardly any attention. We hope the theoretical and the empirical findings in this work will motivate further study in this direction.

References

- [1] Rohit Agrawal and Thibaut Horel. Optimal bounds between f-divergences and integral probability metrics. In *Proceedings of the 37th International Conference on Machine Learning*, 2020.
- [2] Martial Agueh and Guillaume Carlier. Barycenters in the wasserstein space. *SIAM Journal on Mathematical Analysis*, 43(2):904–924, 2011.
- [3] Jason Altschuler, Francis Bach, Alessandro Rudi, and Jonathan Niles-Weed. Massively scalable Sinkhorn distances via the Nyström method. In *NeurIPS*, 2019.
- [4] Jason Altschuler, Jonathan Weed, and Philippe Rigollet. Near-linear time approximation algorithms for optimal transport via Sinkhorn iteration. In *NeurIPS*, 2017.
- [5] Radu Ioan Bot. *Conjugate Duality in Convex Optimization*, volume 637 of *Lecture Notes in Economics and Mathematical Systems book series*. Springer, 2010.

- [6] Leon Bottou, Martin Arjovsky, David Lopez-Paz, and Maxime Oquab. Geometrical insights for implicit generative modeling. *arXiv preprint arXiv:1712.07822*, 2017.
- [7] Stephen Boyd and Lieven Vandenbergh. *Convex optimization*. Cambridge university press, 2004.
- [8] L. Chizat, G. Peyre, B. Schmitzer, and F.-X. Vialard. Unbalanced optimal transport: Dynamic and kantorovich formulations. *Journal of Functional Analysis*, 274(11):3090–3123, 2018.
- [9] Lenaïc Chizat. Unbalanced optimal transport : Models, numerical methods, applications. Technical report, Universite Paris sciences et lettres, 2017.
- [10] Lenaïc Chizat, Gabriel Peyré, Bernhard Schmitzer, and François-Xavier Vialard. Scaling algorithms for unbalanced optimal transport problems. *Math. Comput.*, 87(314):2563–2609, 2018.
- [11] N. Courty, R. Flamary, D. Tuia, and A. Rakotomamonjy. Optimal transport for domain adaptation. *IEEE Transactions on Pattern Analysis and Machine Intelligence*, 39(9):1853–1865, 2017.
- [12] Nicolas Courty, Rémi Flamary, Amaury Habrard, and Alain Rakotomamonjy. Joint distribution optimal transportation for domain adaptation. In *Advances in Neural Information Processing Systems*, volume 30, pages 3730–3739, 2017.
- [13] Marco Cuturi. Sinkhorn distances: Lightspeed computation of optimal transport. In *Proceedings of the 26th International Conference on Neural Information Processing Systems - Volume 2*, page 2292–2300, 2013.
- [14] Marco Cuturi and Arnaud Doucet. Fast computation of wasserstein barycenters. In *Proceedings of the 31st International Conference on International Conference on Machine Learning - Volume 32*, page II–685–II–693. JMLR.org, 2014.
- [15] Bharath Bhushan Damodaran, Benjamin Kellenberger, Rémi Flamary, Devis Tuia, and Nicolas Courty. Deepjdot: Deep joint distribution optimal transport for unsupervised domain adaptation, 2018.
- [16] Dheeru Dua and Casey Graff. UCI machine learning repository, 2017.
- [17] Kilian Fatras, Thibault Séjourné, Nicolas Courty, and Rémi Flamary. Unbalanced minibatch optimal transport; applications to domain adaptation. In *Proceedings of the 38th International Conference on Machine Learning*, 2021.
- [18] Jean Feydy, Thibault Séjourné, François-Xavier Vialard, Shun ichi Amari, Alain Trounev, and Gabriel Peyré. Interpolating between optimal transport and mmd using sinkhorn divergences. In *International Conference on Artificial Intelligence and Statistics*, 2018.
- [19] Charlie Frogner, Chiyuan Zhang, Hossein Mobahi, Mauricio Araya-Polo, and Tomaso Poggio. Learning with a wasserstein loss. In *Proceedings of the 28th International Conference on Neural Information Processing Systems - Volume 2*, pages 2053–2061, 2015.
- [20] Yaroslav Ganin, Evgeniya Ustinova, Hana Ajakan, Pascal Germain, Hugo Larochelle, François Laviolette, Mario Marchand, and Victor Lempitsky. Domain-adversarial training of neural networks. *The journal of machine learning research*, 17(1):2096–2030, 2016.
- [21] Aude Genevay, Lénaïc Chizat, Francis Bach, Marco Cuturi, and Gabriel Peyré. Sample complexity of sinkhorn divergences. In *The 22nd International Conference on Artificial Intelligence and Statistics, AISTATS 2019, 16-18 April 2019, Naha, Okinawa, Japan*, pages 1574–1583, 2019.
- [22] Tryphon T. Georgiou, Johan Karlsson, and Mir Shahrouz Takyar. Metrics for power spectra: An axiomatic approach. *IEEE Transactions on Signal Processing*, 57(3):859–867, 2009.
- [23] Alexandre Gramfort, Gabriel Peyré, and Marco Cuturi. Fast optimal transport averaging of neuroimaging data. In *Proceedings of 24th International Conference on Information Processing in Medical Imaging*, 2015.
- [24] Leonid G. Hanin. Kantorovich-rubinstein norm and its application in the theory of lipschitz spaces. In *PROCEEDINGS OF THE AMERICAN MATHEMATICAL SOCIETY*, volume 115, 1992.
- [25] J.J. Hull. A database for handwritten text recognition research. *IEEE Transactions on Pattern Analysis and Machine Intelligence*, 16(5):550–554, 1994.
- [26] Arun Iyer, Saketha Nath, and Sunita Sarawagi. Maximum mean discrepancy for class ratio estimation. In *ICML*, 2014.
- [27] Aleksandra. A. Kolodziejczyk, Jong Kyoung Kim, Valentine Svensson, John. C. Marioni, and Sarah. A. Teichmann. The technology and biology of single-cell rna sequencing. *Molecular Cell*, 58(4):610–620, 2015.
- [28] Yann LeCun and Corinna Cortes. MNIST handwritten digit database. <http://yann.lecun.com/exdb/mnist/>, 2010.

- [29] Matthias Liero, Alexander Mielke, and Giuseppe Savaré. Optimal transport in competition with reaction: The hellinger-kantorovich distance and geodesic curves. *SIAM J. Math. Anal.*, 48:2869–2911, 2016.
- [30] Matthias Liero, Alexander Mielke, and Giuseppe Savaré. Optimal entropy-transport problems and a new hellinger-kantorovich distance between positive measures. *Inventiones mathematicae*, 211(3):969–1117, 2018.
- [31] Gonzalo Mena and Jonathan Niles-Weed. Statistical bounds for entropic optimal transport: sample complexity and the central limit theorem. In H. Wallach, H. Larochelle, A. Beygelzimer, F. d’Alché-Buc, E. Fox, and R. Garnett, editors, *Advances in Neural Information Processing Systems*, volume 32. Curran Associates, Inc., 2019.
- [32] Kevin R. Moon, David van Dijk, Zheng Wang, Scott Gigante, Daniel B. Burkhardt, William S. Chen, Kristina Yim, Antonia van den Elzen, Matthew J. Hirn, Ronald R. Coifman, Natalia B. Ivanova, Guy Wolf, and Smita Krishnaswamy. Visualizing structure and transitions for biological data exploration. *Nature Biotechnology*, 37(12):1482–1492, 2019.
- [33] Krikamol Muandet, Kenji Fukumizu, Bharath Sriperumbudur, and Bernhard Schölkopf. Kernel mean embedding of distributions: A review and beyond. *Foundations and Trends® in Machine Learning*, 10(1-2):1–141, 2017.
- [34] Alfred Muller. Integral probability metrics and their generating classes of functions. *Advances in Applied Probability*, 29:429–443, 1997.
- [35] Jagarlapudi Saketha Nath and Pratik Kumar Jawanpuria. Statistical optimal transport posed as learning kernel embedding. In *Advances in Neural Information Processing Systems*, 2020.
- [36] Yuval Netzer, Tiejie Wang, Adam Coates, A. Bissacco, Bo Wu, and A. Ng. Reading digits in natural images with unsupervised feature learning. In *NeurIPS*, 2011.
- [37] Xingchao Peng, Ben Usman, Neela Kaushik, Judy Hoffman, Dequan Wang, and Kate Saenko. Visda: The visual domain adaptation challenge. *arXiv preprint arXiv:1710.06924*, 2017.
- [38] Gabriel Peyré and Marco Cuturi. Computational optimal transport. *Foundations and Trends® in Machine Learning*, 11(5-6):355–607, 2019.
- [39] Benedetto Piccoli and Francesco Rossi. Generalized wasserstein distance and its application to transport equations with source. *Archive for Rational Mechanics and Analysis*, 211:335–358, 2014.
- [40] Benedetto Piccoli and Francesco Rossi. On properties of the generalized wasserstein distance. *Archive for Rational Mechanics and Analysis*, 222, 12 2016.
- [41] Geoffrey Schiebinger, Jian Shu, Marcin Tabaka, Brian Cleary, Vidya Subramanian, Aryeh Solomon, Joshua Gould, Siyan Liu, Stacie Lin, Peter Berube, Lia Lee, Jenny Chen, Justin Brumbaugh, Philippe Rigollet, Konrad Hochedlinger, Rudolf Jaenisch, Aviv Regev, and Eric S. Lander. Optimal-transport analysis of single-cell gene expression identifies developmental trajectories in reprogramming. *Cell*, 176(4):928–943.e22, 2019.
- [42] Vivien. Seguy, Bharath B. Damodaran, Remi Flamary, Nicolas Courty, Antoine Rolet, and Mathieu Blondel. Large-scale optimal transport and mapping estimation. In *International Conference on Learning Representations (ICLR)*, 2018.
- [43] Justin Solomon, Fernando de Goes, Gabriel Peyré, Marco Cuturi, Adrian Butscher, Andy Nguyen, Tao Du, and Leonidas Guibas. Convolutional wasserstein distances: Efficient optimal transportation on geometric domains. *ACM Trans. Graph.*, 34(4), 2015.
- [44] Justin Solomon, Raif Rustamov, Leonidas Guibas, and Adrian Butscher. Wasserstein propagation for semi-supervised learning. In Eric P. Xing and Tony Jebara, editors, *Proceedings of the 31st International Conference on Machine Learning*, volume 32 of *Proceedings of Machine Learning Research*, pages 306–314, 2014.
- [45] Bharath K. Sriperumbudur, Kenji Fukumizu, Arthur Gretton, Bernhard Schölkopf, and Gert R. G. Lanckriet. On integral probability metrics, phi-divergences and binary classification. *arXiv preprint arXiv:0901.2698*, 2009.
- [46] Bharath K. Sriperumbudur, Kenji Fukumizu, and Gert R. G. Lanckriet. Universality, characteristic kernels and RKHS embedding of measures. *Journal of Machine Learning Research*, 12:2389–2410, 2011.
- [47] Bharath K. Sriperumbudur, Kenji Fukumizu, and Gert R. G. Lanckriet. Universality, characteristic kernels and rkhs embedding of measures. *J. Mach. Learn. Res.*, 12(null):2389–2410, jul 2011.
- [48] I. Tolstikhin, B. Sriperumbudur, and K. Muandet. Minimax estimation of kernel mean embeddings. *arxiv*, 2016.
- [49] Alexander Tong, Jessie Huang, Guy Wolf, David Van Dijk, and Smita Krishnaswamy. TrajectoryNet: A dynamic optimal transport network for modeling cellular dynamics. In Hal Daumé III and Aarti Singh, editors, *Proceedings of the 37th International Conference on Machine Learning*, volume 119 of *Proceedings of Machine Learning Research*, pages 9526–9536. PMLR, 13–18 Jul 2020.

- [50] C. Villani. *Topics in Optimal Transportation Theory*, volume 58 of *Graduate Studies in Mathematics*. American Mathematical Society, 01 2003.
- [51] A. Wagner, A. Regev, and N. Yosef. Revealing the vectors of cellular identity with single-cell genomics. *Nature Biotechnology*, 34:1145–1160, 2016.
- [52] K. Zhang, B. Scholkopf, K. Muandet, and Z. Wang. Domain adaptation under target and conditional shift. In *ICML*, 2013.

A Proof of Theorem 3.1

To simplify notation, in this proof let $\mathcal{U} \equiv \mathcal{U}_{\mathcal{G},c,\lambda,1,q}$. It is easy to see that \mathcal{U} satisfies the following properties by simple inheritance:

1. $\mathcal{U} \geq 0$. Indeed, each of the objective terms in (5) is non-negative.
2. $\mathcal{U}(s_0, t_0) = 0 \iff s_0 = t_0$. By above observation, sum of non-negative terms is zero if and only if each is zero. Since each term is a metric we have the result.
3. $\mathcal{U}(s_0, t_0) = \mathcal{U}(t_0, s_0)$. Indeed, each objective term in (6) is symmetric.
4. $\mathcal{U}(\rho s_0, \rho t_0) = \rho \mathcal{U}(s_0, t_0)$, $\rho \geq 0$. Follows by change of variables $(s, t) \mapsto (\rho s, \rho t)$ in (6) for $\mathcal{U}(\rho s_0, \rho t_0)$ and $\gamma_{\mathcal{G}}$ being a norm-induced metric satisfies the same property.
5. $\mathcal{U}(s_0, t_0) = u(|s_0 - t_0|)$ for some appropriate function u . Indeed, each objective term in (6) is pointwise maximum of linear functions in $s - t$, hence a shift of variables $(s, t) \mapsto (s + r, t + r)$ shows $\mathcal{U}(s_0, t_0) = \mathcal{U}(s_0 + r, t_0 + r)$.

Towards proving the triangle inequality, we first observe that the q^{th} root of the objective in (6) can be written as $h(x) \equiv \|(h_1(x), h_2(x), h_3(x))\|_q$, where $x \equiv (s, t, s_0, t_0)$. Now, each h_i is pointwise maximum of linear functions in x as each is either W_1 or $\gamma_{\mathcal{G}}$. Domains of h_i are also convex. Hence each h_i is convex. By convexity preserving vector composition rules (for e.g., Section 3.2.4 in [7], we have that $h(x)$ is also convex. Indeed, $h_i \geq 0$ are convex and $\|\cdot\|_q$ is convex and non-increasing in each entry over non-negative orthant. Now, since $\mathcal{U}(s_0, t_0) = \min_{s,t} h(s, t, s_0, t_0)$, where h is convex, we have that \mathcal{U} is also convex (see for e.g., Section 3.2.5 in [7]).

Since \mathcal{U} is convex and positively homogeneous, it is sub-additive. $u(|s_0 - t_0|) = \mathcal{U}(s_0, t_0) = \mathcal{U}(s_0 + r_0, t_0 + r_0) \leq \mathcal{U}(s_0, r_0) + \mathcal{U}(r_0, t_0) = u(|s_0 - r_0|) + u(|r_0 - t_0|)$. Hence \mathcal{U} is a norm-induced metric.

B Proof of Theorem 3.3

We present a proof based on the classical Moreau-Rockafellar formula [5]:

Theorem B.1. *Let X be a real Banach space and $f, g : X \mapsto \mathbb{R} \cup \{\infty\}$ be closed convex functions such that $\text{dom}(f) \cap \text{dom}(g)$ is not empty, then: $(f + g)^*(y) = \min_{x_1 + x_2 = y} f^*(x_1) + g^*(x_2) \forall y \in X^*$. Here, f^* is the Fenchel conjugate of f and X^* is the topological dual space of X .*

Consider the indicator function $F_c : \mathcal{C}(\mathcal{X} \times \mathcal{X}) \mapsto \mathbb{R} \cup \{\infty\}$ defined by: $F_c(f, g) = 0$ if $f(x) + g(y) \leq c(x, y) \forall x, y \in \mathcal{X}$, and ∞ otherwise. Consider another indicator function: $F_{\mathcal{G}}(f, g)$ defined as: 0 if $f \in \mathcal{G}, g \in \mathcal{G}$ and ∞ otherwise. Topological dual of $\mathcal{C}(\mathcal{X} \times \mathcal{X})$ is regular Radon measures $\mathcal{R}(\mathcal{X} \times \mathcal{X})$ and the duality product $\langle h, \pi \rangle \equiv \int h d\pi$.

Now, it is easy to see that $F_c^*(s, t) = \max_{f \in \mathcal{C}(\mathcal{X}), g \in \mathcal{C}(\mathcal{X})} \int f ds + \int g dt$, s.t. $f(x) + g(y) \leq c(x, y) \forall x, y \in \mathcal{X}$, which under the assumptions that \mathcal{X} is compact and c is continuous, is Wasserstein $W(s, t)$ with cost c [50]. On the other hand, $F_{\mathcal{G}(\lambda)}^*(s, t) = \lambda (\max_{f \in \mathcal{G}} \int f ds + \max_{g \in \mathcal{G}} \int g dt) = \lambda (\gamma_{\mathcal{G}}(s, 0) + \gamma_{\mathcal{G}}(t, 0))$. Note that $\mathcal{U}_{\mathcal{G},c,\lambda,1,1}(s_0, t_0) = \min_{(s,t)+(s_1,t_1)=(s_0,t_0)} F_c^*(s, t) + F_{\mathcal{G}(\lambda)}^*(s_1, t_1)$.

Now, observe that $F_{\mathcal{G}}$ is a closed, convex function because \mathcal{G} is a closed, convex set. On the other hand, F_c is trivially convex and is closed because c is continuous. Hence by applying the Moreau-Rockafellar formula we have that:

$$\mathcal{U}_{\mathcal{G},c,\lambda,1,1}(s_0, t_0) = \max_{f \in \mathcal{G}(\lambda), g \in \mathcal{G}(\lambda)} \int f ds + \int g dt, \text{ s.t. } f(x) + g(y) \leq c(x, y) \forall x, y \in \mathcal{X} \quad (12)$$

Now, the constraints in (12) are equivalent to: $g(y) \leq \min_{x \in \mathcal{X}} c(x, y) - f(x) \forall y \in \mathcal{X}$. The RHS is nothing but the c -conjugate (c -transform) of f . From proposition 6 in [38], whenever c is a metric, we have: $\min_{x \in \mathcal{X}} d(x, y) - f(x) = \begin{cases} -f(y) & \text{if } f \in \mathcal{W}_c, \\ -\infty & \text{otherwise.} \end{cases}$ Thus the constraints are equivalent to: $g(y) \leq -f(y) \forall y \in \mathcal{X}, f \in \mathcal{W}_c$. By symmetry, we also obtain that $f(y) \leq -g(y) \forall y \in \mathcal{X}, g \in \mathcal{W}_c$. Now, since the dual, (12), seeks to maximize the objective with respect to g , and monotonically increases with values of g ; at optimality we have that $g(y) = -f(y) \forall y \in \mathcal{X}$. Note that this equality is possible to achieve as both $g, f \in \mathcal{G}(\lambda) \cap \mathcal{W}_c$. Eliminating g , one obtains (7).

C Proof of theorem 3.6

It is straight-forward to show all the metric properties except the triangle inequality. To simplify notation we denote $\mathcal{U}(\mathcal{G}, c, \lambda, p, 1)$ by \mathcal{U} . Also, we assume all measures involved admit (un-normalized) densities merely to simplify

notation. Analogous derivations hold for those in $\mathcal{R}^+(\mathcal{X})$. To prove the triangle inequality, we need to show that $\mathcal{U}(r_0, t_0) \leq \mathcal{U}(r_0, s_0) + \mathcal{U}(s_0, t_0)$ holds.

Let r_1, s_1 be the optimal solution in (6) that defines $\mathcal{U}(r_0, s_0)$. Likewise, Let s_2, t_2 be the optimal solution in (6) that defines $\mathcal{U}(s_0, t_0)$. Now if $s_1 = s_2$, then the triangle inequality trivially follows from that of $W_p, \gamma_{\mathcal{M}_k}$ (inheritance). Now, let's assume that $s_1 \neq s_2$. We invoke the gluing lemma style argument for this case.

Define the gluing marginal $\bar{s} \equiv \min(s_1, s_2)$. Let π_1, π_2 denote the optimal transport plans for $W_p(r_1, s_1), W_p(s_2, t_2)$ respectively. Let \bar{r}, \bar{t} be the projections of \bar{s} onto π_1, π_2 respectively i.e., $\bar{r}(x) = \int \pi_1(x/y) \bar{s}(y) dy$ and $\bar{t}(z) = \int \pi_2(z/y) \bar{s}(y) dy$. Let $\bar{\pi}_1(x, y) \equiv \pi_1(x/y) \bar{s}(y)$ and $\bar{\pi}_2(x, y) \equiv \pi_2(x/y) \bar{s}(y)$. Since by definition $\bar{\pi}_i \leq \pi_i$, we have that $|\bar{s}|W_p(\bar{r}, \bar{s}) \leq |s_1|W_p(r_1, s_1)$ and $|\bar{s}|W_p(\bar{s}, \bar{t}) \leq |s_2|W_p(s_2, t_2)$. However, as we shall observe later, these trivial upper bounds are not enough to show triangle inequality with IPM regularization⁴. Here we will need more tighter upper bounds, which can be obtained in view of the assumptions in the theorem statement. To this end, we present the following lemma:

Lemma C.1. $|s_1|W_p(r_1, s_1) - |\bar{s}|W_p(\bar{r}, \bar{s}) \geq \frac{r^p |s_1 - \bar{s}|_{TV}}{pR^{p-1}}$. Analogously, $|s_2|W_p(s_2, t_2) - |\bar{s}|W_p(\bar{s}, \bar{t}) \geq \frac{r^p |s_2 - \bar{s}|_{TV}}{pR^{p-1}}$.

Proof. Let $a^p \equiv |s_1|W_p(r_1, s_1), b^p \equiv |\bar{s}|W_p(\bar{r}, \bar{s})$. Now, $a^p - b^p \geq \int \mathbb{E}_{\pi_1(\cdot/y)} [c^p(X, y)/y] (s_1(y) - \bar{s}(y)) dy \geq r^p |s_1 - \bar{s}|_{TV}$. This is because we assume the cost is lower bounded by r and $\pi_1(x/y)$ is a probability density. Likewise, $b \leq a \leq R|s_1|^{1/p}$. Hence, $\sum_{i=0}^{p-1} a^i b^{p-1-i} \leq pR^{p-1}|s_1|^{\frac{p-1}{p}}$. Again, this is because the cost is upper bounded by R . Now, $|s_1|^{1/p}W_p(r_1, s_1) - |\bar{s}|^{1/p}W_p(\bar{r}, \bar{s}) = a - b = \frac{a^p - b^p}{\sum_{i=0}^{p-1} a^i b^{p-1-i}} \geq \frac{r^p |s_1 - \bar{s}|_{TV}}{pR^{p-1}|s_1|^{\frac{p-1}{p}}}$. Multiplying this final inequality

by $|s_1|^{\frac{p-1}{p}}$ and observing that $|\bar{s}| \leq |s_1|$ gives the required inequality. \square

Now, since $s_1 \neq s_2$, we have that $|s_i - \bar{s}|_{TV} > 0$ and the lower bound in lemma C.1 is (strictly) positive. While lemma C.1 lower bounds the improvement in the Wasserstein term by employing the gluing marginal, the following lemma upper bounds the slack introduced in the IPM terms because of the same:

Lemma C.2. $(\gamma_{\mathcal{G}}(r_0, \bar{r}) + \gamma_{\mathcal{G}}(t_0, \bar{t})) - (\gamma_{\mathcal{G}}(r_0, r_1) + \gamma_{\mathcal{G}}(t_0, t_2)) \leq \beta |s_1 - s_2|_{TV}$.

Proof. Recall that $\bar{r}(x) \equiv \int \pi_1(x/y) \bar{s}(y) dy = \int_{y:s_1(y) \leq s_2(y)} \pi_1(x/y) s_1(y) dy + \int_{y:s_1(y) > s_2(y)} \pi_1(x/y) s_2(y) dy = \int \pi_1(x/y) s_1(y) dy + \int_{y:s_1(y) > s_2(y)} \pi_1(x/y) (s_2(y) - s_1(y)) dy = r_1(x) + \int_{y:s_1(y) > s_2(y)} \pi_1(x/y) (s_2(y) - s_1(y)) dy$. The last equality is because π_1 is the optimal plan for $W_p(r_1, s_1)$. Now subtracting both sides by $r_0(x)$ and equating the IPM value for both the sides gives: $\gamma_{\mathcal{G}}(r_0, \bar{r}) = \max_{f \in \mathcal{G}} \left(\int f(x) (r_0(x) - r_1(x)) dx + \int_{y:s_1(y) > s_2(y)} f(x) \pi_1(x/y) (s_1(y) - s_2(y)) dy \right) \leq \gamma_{\mathcal{G}}(r_0, r_1) + \max_{f \in \mathcal{G}} \int_{y:s_1(y) > s_2(y)} \mathbb{E}_{\pi_1(\cdot/y)} [f(X)/y] (s_1(y) - s_2(y)) dy$. Now, by the assumption on \mathcal{G} we have that $|f(x)| \leq \beta \Rightarrow \mathbb{E}_{\pi_1(\cdot/y)} [f(X)/y] \leq \beta$. Hence, $\gamma_{\mathcal{G}}(r_0, \bar{r}) \leq \gamma_{\mathcal{G}}(r_0, r_1) + \beta \int_{y:s_1(y) > s_2(y)} (s_1(y) - s_2(y)) dy$. Similarly, we obtain $\gamma_{\mathcal{G}}(t_0, \bar{t}) \leq \gamma_{\mathcal{G}}(t_0, t_2) + \beta \int_{y:s_1(y) \leq s_2(y)} (s_2(y) - s_1(y)) dy$. Adding these two gives the required inequality. \square

We are now ready to prove the triangle inequality:

$$\begin{aligned} \mathcal{U}(r_0, t_0) &\leq |\bar{s}|W_p(\bar{r}, \bar{t}) + \lambda \gamma_{\mathcal{G}}(r_0, \bar{r}) + \lambda \gamma_{\mathcal{G}}(t_0, \bar{t}) \\ &\leq |\bar{s}|W_p(\bar{r}, \bar{s}) + |\bar{s}|W_p(\bar{s}, \bar{t}) + \lambda \gamma_{\mathcal{G}}(r_0, \bar{r}) + \lambda \gamma_{\mathcal{G}}(t_0, \bar{t}) \\ &\leq |s_1|W_p(r_1, s_1) + |s_2|W_p(s_2, t_2) + \lambda \gamma_{\mathcal{G}}(r_0, \bar{r}) + \lambda \gamma_{\mathcal{G}}(t_0, \bar{t}) - \frac{r^p}{pR^{p-1}} |s_2 - s_1|_{TV} \\ &\leq |s_1|W_p(r_1, s_1) + |s_2|W_p(s_2, t_2) + \lambda \gamma_{\mathcal{G}}(r_0, r_1) + \lambda \gamma_{\mathcal{G}}(t_0, t_2) + \left(\lambda \beta - \frac{r^p}{pR^{p-1}} \right) |s_2 - s_1|_{TV} \\ &\leq \mathcal{U}(r_0, s_0) + \mathcal{U}(s_0, t_0) \end{aligned}$$

Here, the first inequality is by definition of $\mathcal{U}(r_0, t_0)$ in (6). Second is true because W_p is a metric. Third is true because of Lemma C.1 and the fact that Total Variation is a metric. The fourth is because of Lemma C.2. The last follows from the upper bound on λ and adding the required terms.

⁴In case of Total Variation regularization, these inequalities are sufficient to prove the triangle inequality [39].

D Proof of Theorem 3.10

Recalling the definition of \bar{U} :

$$\bar{U}(s_0, t_0) \equiv \min_{\pi \in \mathcal{R}_1^+(\mathcal{X} \times \mathcal{X})} h(\pi, s_0, t_0) \equiv \left(\int c^p d\pi \right)^{1/p} + \lambda \gamma_{\mathcal{G}}(\pi_1, s_0) + \lambda \gamma_{\mathcal{G}}(\pi_2, t_0),$$

Now, we have:

$$\begin{aligned} \bar{U}(\hat{s}_m, \hat{t}_m) - \bar{U}(s_0, t_0) &= \min_{\pi \in \mathcal{R}_1^+(\mathcal{X} \times \mathcal{X})} h(\pi, \hat{s}_m, \hat{t}_m) - \min_{\pi \in \mathcal{R}_1^+(\mathcal{X} \times \mathcal{X})} h(\pi, s_0, t_0) \\ &\leq h(\pi^*, \hat{s}_m, \hat{t}_m) - h(\pi^*, s_0, t_0) \quad (\text{where } \pi^* = \arg \min_{\pi \in \mathcal{R}_1^+(\mathcal{X} \times \mathcal{X})} h(\pi, s_0, t_0)) \\ &= \lambda (\gamma_{\mathcal{G}}(\pi_1^*, \hat{s}_m) - \gamma_{\mathcal{G}}(\pi_1^*, s_0) + \gamma_{\mathcal{G}}(\pi_2^*, \hat{t}_m) - \gamma_{\mathcal{G}}(\pi_2^*, t_0)) \\ &\leq \lambda (\gamma_{\mathcal{G}}(s_0, \hat{s}_m) + \gamma_{\mathcal{G}}(t_0, \hat{t}_m)) \quad (\because \gamma \text{ satisfies triangle inequality}) \end{aligned}$$

The existence of π^* is guaranteed as h is continuous wrt. π and $\mathcal{R}_1^+(\mathcal{X} \times \mathcal{X})$ is a compact set. Similarly, one can show that

$$\begin{aligned} -(\bar{U}(\hat{s}_m, \hat{t}_m) - \bar{U}(s_0, t_0)) &\leq \lambda (\gamma_{\mathcal{G}}(s_0, \hat{s}_m) + \gamma_{\mathcal{G}}(t_0, \hat{t}_m)) \\ \implies |\bar{U}(\hat{s}_m, \hat{t}_m) - \bar{U}(s_0, t_0)| &\leq \lambda (\gamma_{\mathcal{G}}(s_0, \hat{s}_m) + \gamma_{\mathcal{G}}(t_0, \hat{t}_m)) \end{aligned}$$

The rate at which LHS goes to zero is hence same as that with which either of the IPM terms goes to zero. For example, if the IPM is MMD with a normalized kernel, then $\gamma_{\mathcal{M}_k}(s_0, \hat{s}_m) \leq \sqrt{\frac{1}{m}} + \sqrt{\frac{2 \log(1/\delta)}{m}}$ with probability $1 - \delta$ [48].

From the union bound, with probability $1 - \delta$, $\text{LHS} \leq 2\lambda \left(\sqrt{\frac{1}{m}} + \sqrt{\frac{2 \log(2/\delta)}{m}} \right)$. Thus, $O\left(\frac{1}{\sqrt{m}}\right)$ is the common bound for the rate at which the LHS as well as $\gamma_{\mathcal{M}_k}(s_0, \hat{s}_m)$ decay to zero. In summary, the proposed metrics inherit their sample complexity from the IPM regularizers rather than from the Wasserstein metrics.

E Experiments

We present more experimental details and additional results in this section. We will open-source the codes to reproduce all our experiments upon acceptance of the paper.

E.1 Synthetic Experiments

Effect of Regularization We experiment on synthetic data with a bimodal distribution and observe the effect of regularization on the transport plans of the proposed method. Figure 3 shows marginals of transport plans with normalized measures (balanced case) and un-normalized measures (unbalanced case) respectively. The source and target measures are shown using dashed lines and plans are the filled plots. On increasing regularization, the match between marginals of the transport plan and the given source and target marginals become better. Euclidean distance is used as the ground cost metric and the regularization is squared-MMD. The proposed method is solved using Projected Gradient Descent with Armijo rule for step-size selection. IMQ kernel with hyper-parameter K^2 as 10^{-6} is used in all our results.

Barycenter with Gaussian measures We experiment with source and target measures as Gaussian and compare our barycenters with those obtained with MMD and ϵ KL-UOT. The rows in 4 are for the case with normalized and un-normalized Gaussian measures respectively. Interpolation by MMD is the empirical average of two measures and is denoted by Avg. The proposed method is solved using Mirror Descent with step-size as the inverse of infinity norm of gradient. Sinkhorn-stabilized barycenter solver from the Python-OT (POT) library are used for OT and ϵ KL-UOT.

Level Sets with the Proposed Metric Mirror Descent with step-size as the inverse of infinity norm of gradient is run for 100 iterations for solving the proposed method. For plotting contour plots, the hyper-parameter specifying total number of lines is 20 for all methods.

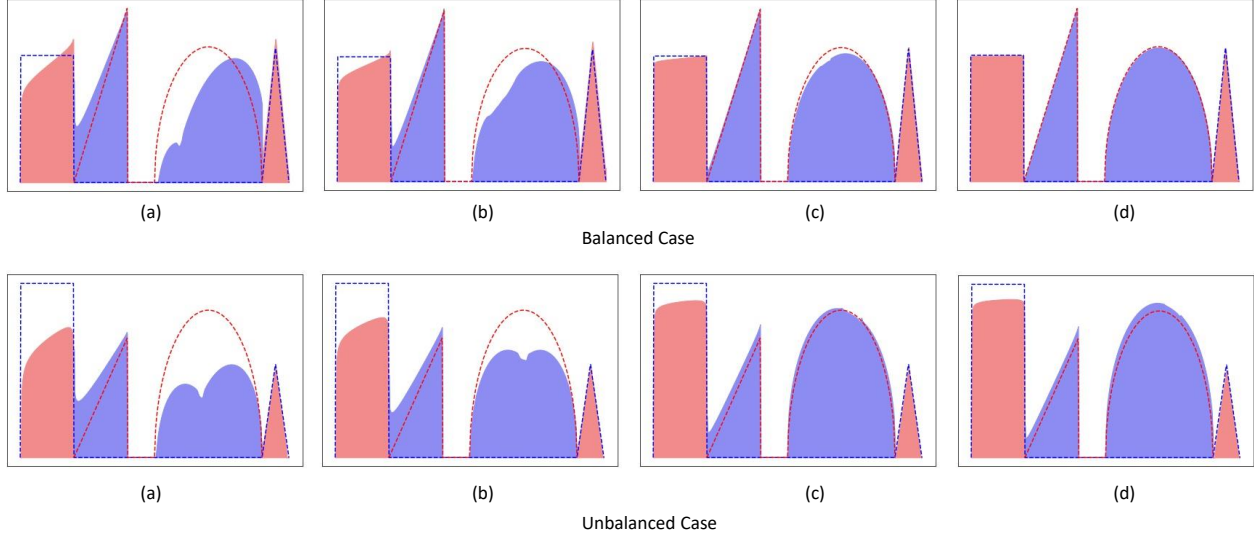


Figure 3: Effect of increasing regularization in Synthetic Bimodal example

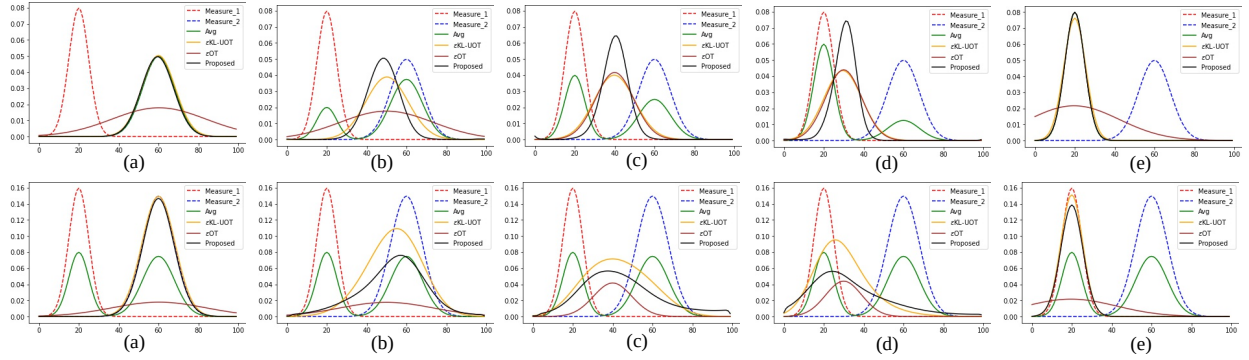


Figure 4: Barycenter with Gaussian Measures. The first row is with normalized measures and the second row is with un-normalized measures.

E.2 Single cell RNA sequencing

Embryoid Body dataset comprises of data at 5 timesteps with sample sizes as 2381, 4163, 3278, 3665 and 3332 respectively. For the task of prediction at timestep t_i , the data was standardized using statistics of data from $\{t_0, t_1, t_2, t_3, t_4\} \setminus \{t_i\}$. Mirror Descent is used to solve the barycenter formulations for the proposed method as well as for ϵ KL-UOT, with step size as the inverse of infinity norm of the gradient. During the validation phase, 100 iterations of Mirror Descent are performed and for reporting final performance on the chosen hyper-parameters 1000 iterations are performed. For the proposed method, constant K^2 , of the IMQ kernel is chosen from $\{1e-3, 1e-4, 1e-5\}$ and λ is chosen from $\{1, 1e-1, 1e-2\}$. For ϵ KL-UOT, λ is chosen from $\{1, 1e-1, 1e-2\}$ and the coefficient of entropic regularization is chosen from $\{1e-1, 1e-3, 1e-5\}$.

E.3 Domain Adaptation in JUMBOT framework

The accuracies shown in table 3 are averages across three independent trials with the same seed as used by JUMBOT. Mirror Descent with step-size as the inverse of infinity norm of gradient is run for 500 iterations to solve the proposed UOT formulation. For Digits dataset, we additionally added an L2-regularization with coefficient 10 on the transport matrix. The digits experiment is done on NVIDIA RTX 2080 GPU and the VisDA experiment is done on NVIDIA GTX 1080 Ti GPU.

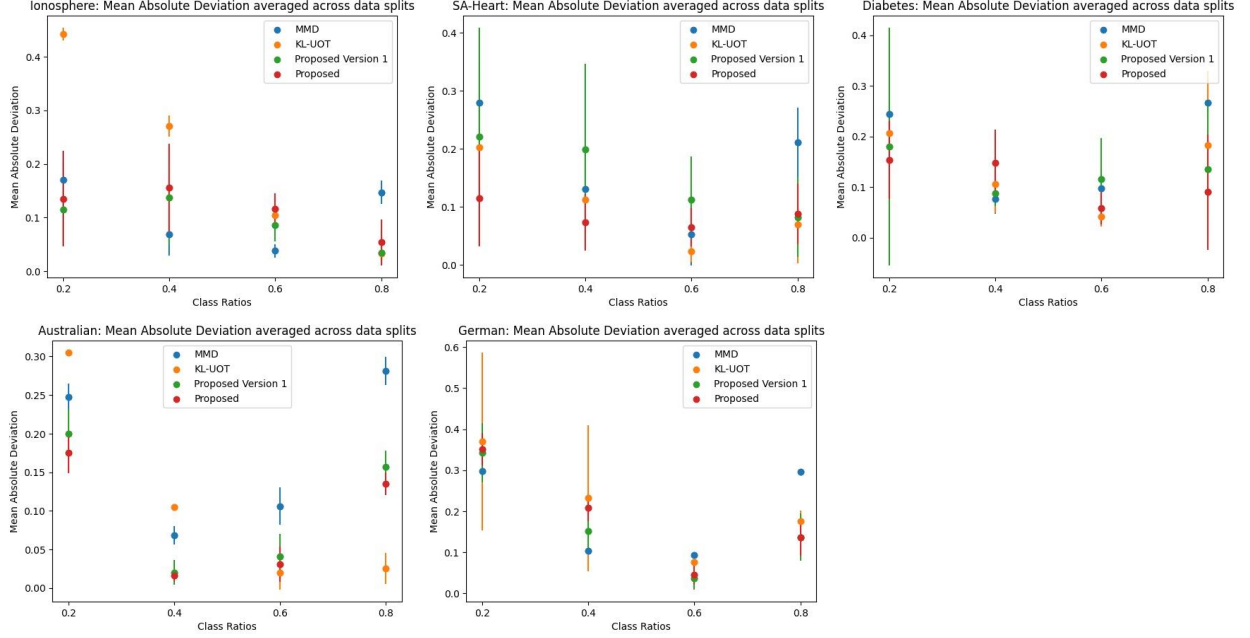


Figure 5: Mean Absolute Deviation averaged across data splits shown separately for each class ratio

Table 4: Mean Absolute Deviation (lesser is better) averaged across data splits

DATASET	MMD	ϵ KL-UOT	PROPOSED VERSION 1	PROPOSED
IONOSPHERE	0.106 \pm 0.027	0.212 \pm 0.013	0.093\pm0.050	0.116 \pm 0.061
SAHEART	0.169 \pm 0.059	0.102 \pm 0.042	0.154 \pm 0.120	0.085\pm0.054
DIABETES	0.171 \pm 0.029	0.134 \pm 0.069	0.129 \pm 0.119	0.112\pm0.072
AUSTRALIAN	0.175 \pm 0.018	0.114 \pm 0.011	0.105 \pm 0.025	0.089\pm0.018
GERMAN	0.198 \pm 0.008	0.214 \pm 0.106	0.167\pm0.053	0.185 \pm 0.035

E.4 Class Ratio Experiment

We experimented on four UCI datasets- Australian, Ionosphere, SA-Heart and Diabetes. We also include results on German Credit data. Based on an initial random seed, we divided the data into a training set and a test set. The (training set size, test set size) for Australian, Ionosphere, SA-Heart, Diabetes and German datasets are (454, 100), (172, 50), (192, 80), (376, 100) and (400, 100) respectively. Hyper-parameters are tuned on 30 validation sets that were randomly sampled from the training set. The ratio of classes in the training sets was kept as 0.5. We report the results on the test set with the best hyper-parameter after repeating the experiment with 4 initial random seeds. All methods are solved using Mirror Descent with step size as the inverse of infinity norm of the gradient. During the validation phase, 500 iterations of Mirror Descent are performed and during the final test phase 1000 iterations are performed.

In the main paper, we presented results with the proposed formulation where we take union of source and target data as the support of the transport matrix. Here, we also present results with the proposed method where the transport matrix is parameterized by source and target samples on the two sides respectively, i.e. $\alpha \in \mathbb{R}^{m_1 \times m_2}$. We refer to it as **proposed version 1**. Table 4 shows that proposed version 1 also performs better than both MMD and ϵ KL-UOT baselines on Three out of the Four datasets. In figure 5, we present the Mean Absolute Deviations averaged across data splits for each class ratio separately.

For proposed version 1 and proposed formulation, λ is chosen from $\{0.1, 1, 10\}$ for Ionosphere dataset, from $\{0.01, 0.1, 1\}$ for Australian and German datasets, from $\{1, 10, 100\}$ for Diabetes dataset and from $\{0.1, 1, 10\}$ for SAHeart dataset. The constant hyper-parameter used in IMQ kernel is chosen from $\{1, 10, 20\}$ for Ionosphere and from $\{100, 150, 200\}$ for all other datasets. The pool of hyper-parameters is chosen based on scale of terms in the involved objective functions and the condition numbers of Gram matrices.

Table 5: Mean Accuracy (in %) after Domain Adaptation (higher is better) averaged across data splits

DATASET	ϵ KL-UOT	PROPOSED VERSION 1	PROPOSED
IONOSPHERE	51.1 \pm 0.063	82.1\pm0.041	80.3 \pm 0.038
SAHEART	57.2 \pm 0.038	57.9\pm0.071	57.8 \pm 0.040
DIABETES	59.3 \pm 0.049	64.5 \pm0.050	63.9 \pm 0.033
AUSTRALIAN	44.2 \pm 0.141	45.2\pm0.125	44.8 \pm 0.124
GERMAN	50.8 \pm 0.046	51.3\pm0.059	51.1 \pm 0.052

For MMD, RBF kernel is used as it resulted in better optimization compared to IMQ kernel. For validation, the pool of σ^2 values was $\{10, 20, 30\}$ for Australian and German datasets, $\{0.01, 0.05, 0.1\}$ for Ionosphere, $\{30, 40, 50\}$ for SA-Heart and $\{30, 40, 50\}$ for Diabetes dataset. The chosen σ^2 values are 20 for Australian, 0.1 for Ionosphere, 50 for SA-Heart and 50 for Diabetes dataset. For German dataset, σ^2 was chosen as 30 for class ratio's 0.2 and 0.4 and it was chosen as 20 for class ratio's 0.6 and 0.8.

For ϵ KL-UOT, λ is chosen from $\{0.1, 0.01, 0.001\}$ for Australian dataset and from $\{1, 0.1, 0.01\}$ for all other datasets. The entropic regularizer, ϵ , is chosen from $\{0.1, 0.01, 0.001\}$. The pool of hyper-parameters is chosen based on the scale of terms in the objective. We note that for the ϵ KL-UOT optimization, optimal θ at iteration k is $\theta_k = [\sum_{i:y_i=0} \alpha_k^\top \mathbf{1}_i, \sum_{i:y_i=1} \alpha_k^\top \mathbf{1}_i]$.

Australian For ϵ KL-UOT, the chosen hyper-parameters (λ, ϵ) for class ratios 0.2, 0.4, 0.6, 0.8 are $(10^{-3}, 10^{-1})$, $(10^{-3}, 10^{-1})$, $(10^{-2}, 10^{-3})$, $(10^{-1}, 10^{-3})$ respectively. For Proposed version 1 method, the chosen hyper-parameters (λ, K^2) for class ratios 0.2, 0.4, 0.6, 0.8 are (1, 200), (1, 200), (0.01, 150), (0.01, 200) respectively. For Proposed, the chosen hyper-parameters (λ, K^2) for class ratios 0.2, 0.4, 0.6, 0.8 are (1, 200), (1, 200), (0.1, 150), (0.01, 200) respectively.

Ionosphere For ϵ KL-UOT, the chosen hyper-parameters (λ, ϵ) for class ratios 0.2, 0.4, 0.6, 0.8 are $(10^{-2}, 10^{-1})$, $(10^{-2}, 10^{-1})$, $(10^{-2}, 10^{-1})$, $(1, 10^{-1})$ respectively. For Proposed version 1 method, the chosen hyper-parameters (λ, K^2) are (10, 1) for all class ratios. For Proposed, the chosen hyper-parameters (λ, K^2) for class ratios 0.2, 0.4, 0.6, 0.8 are (0.1, 10), (0.1, 10), (0.1, 1), (1, 1) respectively.

Diabetes For ϵ KL-UOT, the chosen hyper-parameters (λ, ϵ) for class ratios 0.2, 0.4, 0.6, 0.8 are $(10^{-1}, 10^{-3})$, $(10^{-1}, 10^{-3})$, $(10^{-2}, 10^{-2})$, $(10^{-1}, 10^{-3})$ respectively. For Proposed version 1 method, the chosen hyper-parameters (λ, K^2) for class ratios 0.2, 0.4, 0.6, 0.8 are (10, 200), (1, 100), (1, 150), (1, 200) respectively. For Proposed, the chosen hyper-parameters (λ, K^2) for class ratios 0.2, 0.4, 0.6, 0.8 are (1, 200), (1, 100), (1, 200), (1, 200) respectively.

SAHeart For ϵ KL-UOT, the chosen hyper-parameters (λ, ϵ) for class ratios 0.2, 0.4, 0.6, 0.8 are $(1, 10^{-3})$, $(10^{-2}, 10^{-1})$, $(10^{-2}, 10^{-2})$, $(10^{-2}, 10^{-3})$ respectively. For Proposed version 1 method, the chosen hyper-parameters (λ, K^2) for class ratios 0.2, 0.4, 0.6, 0.8 are (10, 100), (10, 100), (10, 150), (1, 100) respectively. For Proposed, the chosen hyper-parameters (λ, K^2) for class ratios 0.2, 0.4, 0.6, 0.8 are (1, 200), (1, 100), (0.1, 200), (10, 200) respectively.

German For ϵ KL-UOT, the chosen hyper-parameters (λ, ϵ) for class ratios 0.2, 0.4, 0.6, 0.8 are $(1, 10^{-3})$, $(10^{-1}, 10^{-3})$, $(10^{-2}, 10^{-1})$, $(10^{-2}, 10^{-3})$ respectively. For Proposed version 1 method, the chosen hyper-parameters (λ, K^2) for class ratios 0.2, 0.4, 0.6, 0.8 are (1, 100), (1, 100), (0.1, 100), (0.01, 200) respectively. For Proposed, the chosen hyper-parameters (λ, K^2) for class ratios 0.2, 0.4, 0.6, 0.8 are (1, 100), (0.1, 100), (1, 200), (0.01, 200) respectively.

E.4.1 Classification Accuracy

For OT based methods, we further use the transport matrix for getting classification accuracy on test data. To this end, we first compute the Barycentric projection of test data onto source data and label a test point based on the source point nearest to its Barycentric projection. For a sample x , the Barycentric projection of sample x is $T(x) \equiv \operatorname{argmin}_{y \in \mathcal{Y}} \mathbb{E}[c(y, Y)|x]$. In our experiment, $\text{cost } c(\cdot, \cdot)$ is squared-Euclidean.

We note that this classification experiment was performed using the same set of hyper-parameters that were chosen after validating for Mean Absolute Deviation. The results are shown in table 5 where we outperformed the baselines.

E.5 Computation Time

We take the source and the target marginal as the same Gaussian distribution and run the Mirror Descent iterates until the proposed objective is 0. The ground cost is taken as squared-Euclidean and the regularization is squared MMD. The resulting plot is shown in figure 6. Our future work will include making the computation faster.

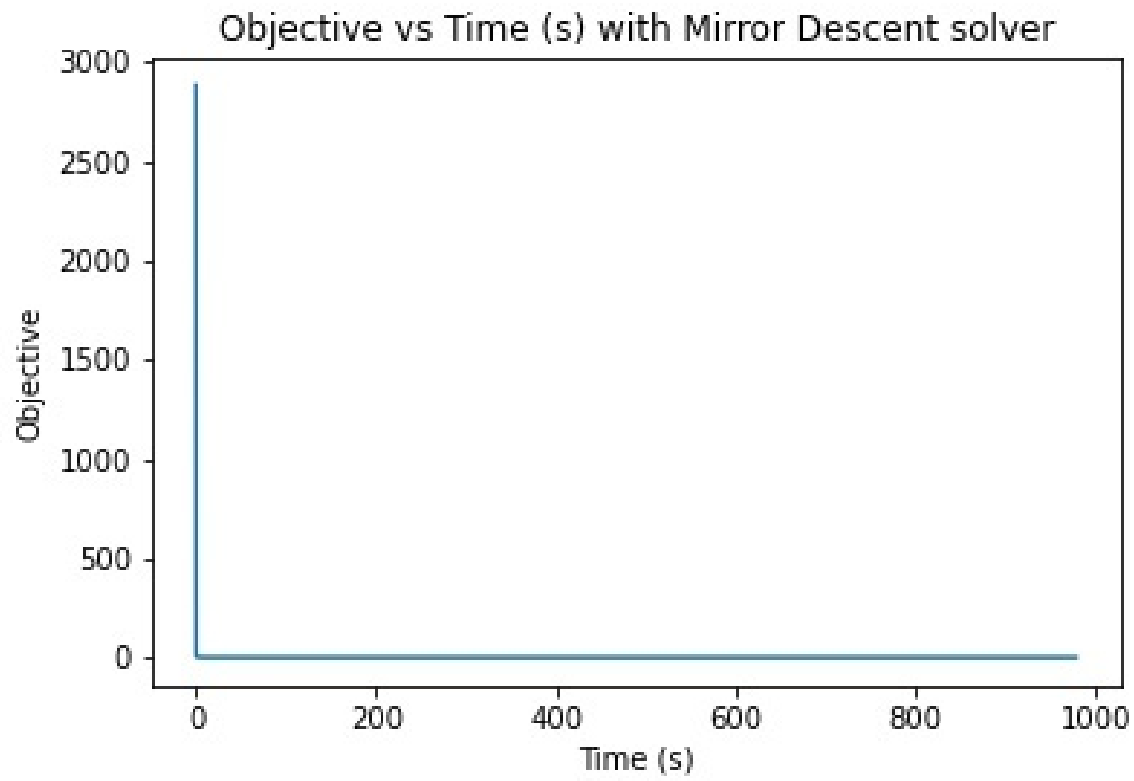


Figure 6: Time(s) for objective to decrease to 0 when the source and target marginals are same